COAL ASH EFFECTS IN THE CORROSION PERFORMANCE OF STRUCTURAL ALLOYS IN SIMULATED OXY-FUEL ENVIRONMENTS

K. Natesan and Z. Zeng
Argonne National Laboratory, 9700 South Cass Avenue, Argonne, IL 60439
E-mail: natesan@anl.gov; Telephone: (630) 252-5103; Fax: (630) 252-8681

Abstract

The U.S. Department of Energy (DOE) Office of Fossil Energy is intensely promoting research and development of oxy-fuel combustion systems that employ oxygen, instead of air, for burning the fuel. The resulting flue gas primarily consists of H_2O and CO_2 that facilitates sequestration of CO_2 or use it in a turbine to generate electricity, thereby leading to a reduction in CO_2 emissions. Also, as the oxidant is bereft of N_2, NO_x emissions are minimized to a great extent from the exhaust gas. Studies at NETL have indicated that oxy-fuel combustion can increase efficiency in the power plants from the current 30-35% to 50-60%. However, the presence of H_2O/CO_2 and trace constituents like sulfur and chlorine in the gas environment and coal ash deposits including alkalis at the operating temperatures and pressures can have adverse effects on the corrosion and mechanical properties of structural alloys. Thus, there is a critical need to evaluate the response of structural and turbine materials in simulated H_2O/CO_2 environments in an effort to select materials that have adequate high temperature mechanical properties and long-term environmental performance.

During the past few years, we have conducted corrosion tests on a variety of candidate alloys in CO_2 and steam containing environments in the presence of SO_2, typical of oxy-fuel combustion systems. Materials selected for the study include intermediate-chromium ferritic steels, Fe-Cr-Ni heat-resistant alloys, and nickel-based superalloys. We presented detailed results on the corrosion performance of various alloys after exposure at 750°C. During the current year, we continued testing of alloys to evaluate their performance in a simulated oxy-fuel environment with the presence of simulated coal ash consisting of alumina, silica, and iron oxide along with sodium and potassium sulfates. In addition, we have examined the role of CaO in the ash (typical of US Western coal ash) in laboratory exposure environments. Detailed results are presented on weight change, scale thickness, internal penetration, microstructural characteristics of corrosion products, and the cracking of scales for the alloys after exposure at 750°C. To establish the role of steam in the exposure environment, tests have also been conducted in environments with and without steam in the oxy-fuel gas atmospheres. Results from these tests are used to address the role of steam in the long-term corrosion performance of alloys. In addition, we have procured welded (using commercial weld practice) plates of select alloys and have initiated their corrosion evaluation in oxy-fuel enviroments.

Background

An increase of carbon dioxide gas in the atmosphere has been identified as one of the major causes of the global climate change and one of the sources of carbon dioxide is the exhaust from fossil fuel fired combustion power plants. Energy production, particularly electricity generation, is expected to continue to increase globally due to population growth and a per capita increase in

energy consumption. To meet the energy needs, fossil fuels (coal, oil, and gas) will play a major part in production even with a projected increase in alternate renewable sources. However, to minimize the carbon dioxide emission, the current systems emphasize its capture from power plants and subsequent sequestration. The oxy-fuel combustion systems (without the diluent nitrogen gas) can enable recycling of the carbon dioxide to the compressor, use of novel gas turbines, and advance reuse. The U.S. Department of Energy/Office of Fossil Energy is supporting the development of combustion systems replacing air with nearly pure oxygen with the goal of achieving a near zero-emission coal-based power system. For this purpose, turbines and combustor technologies that use pure oxygen in fuel combustion are being developed. The major advantage of combustion under pure oxygen is the potential for the separation and capture of CO_2 and for achieving power system efficiencies in the range of 50% to 60%.

In previous years, we evaluated the corrosion performance of candidate materials in CO_2, steam, steam-CO_2 mixtures, and air [1-4]. Materials selected for the study include intermediate-chromium ferritic steels, Fe-Cr-Ni heat-resistant alloys, and nickel-based superalloys. Coupon specimens of several of the alloys were exposed to a pure CO_2 and to CO_2 plus steam environments at temperatures between 650°C and 950°C for times of up to 10,000 h. We have presented detailed results on the corrosion performance of various alloys after exposure at 750°C. The data showed that the weight change for all the alloys was small when tested in all four environments. Among the alloys, Alloy 800 exhibited the most weight gain in all four environments. In general, high nickel and Ni-base alloys exhibited less oxidation than the Fe-base alloys in all exposure environments. The high silicon alloys such as Alloys 330 and 333 showed superior corrosion resistance in a pure CO_2 environment when compared to their performance in CO_2-steam or pure steam environments. The volatilization of silicon oxides in the steam-containing environments may be the cause for this increased corrosion. We also addressed the mechanism for the oxidation of various alloys in these environments and also evaluated the long-term performance of the alloys from the standpoint of scaling and internal penetration. The oxidation test results showed that the total corrosion (scaling plus internal penetration) rates are <0.05 mm/y at 750°C, in the absence of ash or sulfur.

In the past year, we performed corrosion tests to evaluate the corrosion performance of the structural alloys in the presence of simulated U.S. Eastern coal ash consisting of alumina, silica, and iron oxide along with sodium and potassium sulfates. Detailed results were presented on weight change, scale thickness, internal penetration, microstructural characteristics of corrosion products, and cracking of scales for the alloys after exposure at 750°C [5,6]. To establish the role of steam in the exposure environment, tests were also conducted in environments with and without steam in the oxy-fuel gas atmospheres. Results from these tests were used to address the role of steam in the long-term corrosion performance of alloys.

The US Eastern coal ash is rich in iron oxide while the US Western coal ash is rich in calcium oxide. Calcium content in ash is an important parameter that can affect the alloy corrosion. Typically, the calcium content in the ash of US Western coal from PRB and Beulah-Zap are much higher than that in the ash of US Eastern coal (see Figure 1). It is necessary to understand the effect of the calcium content on ash corrosion. On the other hand, $CaCO_3$ is also added to combustion environments (such as fluidized beds) to absorb SO_2 and reduced SO_2 emissions. It is also necessary to understand the reactions role of of CaO and $CaCO_3$ in the corrosion of

structural alloys. After completing our study of the effect of US Eastern coal ash on alloy corrosion in the past year, we conducted experiments to investigate the effect of calcium-containing ash on corrosion.

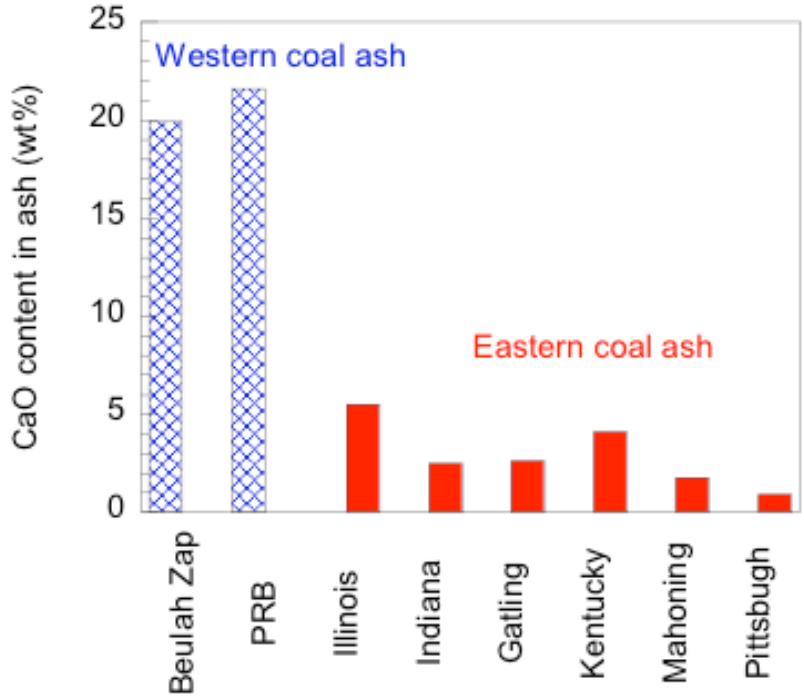

Figure 1. Calcium oxide contents in typical eight US coal ashes

Experimental Procedure

Materials

The compositions of the alloys selected for the study are listed in Table 1. Several alloys, both ASME coded and uncoded, were selected for corrosion evaluation. The alloys included austenitic Fe-base alloys 153MA, 253MA, and Alloy 800H. In addition, several high-Ni alloys (333, 617, 625, 602CA, 230, 693, 740, and 718) were included in the study, especially for application at temperatures above 700°C. MA956 is a Fe-Cr alloy produced via mechanical alloying and subsequent extrusion. Waspalloy and 718 are alloys for turbine applications. Apart from fireside and steam side corrosion resistance, the alloy selected for application in steam superheaters and reheaters should possess adequate strength at elevated temperatures for the duration of service.

Gas composition

Since the concentration of the diluent nitrogen gas in the oxy-fuel combustion systems is very low, the SO_2 concentration in the flue gas of oxy-fuel combustion is generally three to four times higher than that in the flue gas of air combustion. This result is supported by both simulation and actual measurement from recent pilot scale work [7-9]. The effect of a high SO_2 concentration on the alloy corrosion of oxy-fuel combustion systems has been studied by several groups [5-8]. The SO_2 concentrations in these studies varied from 0.32% to 1.5% [10, 11], depending on the

Table 1. Nominal composition (in wt.%) of alloys selected for corrosion study

Material	C	Cr	Ni	Mn	Si	Mo	Fe	Other
153MA	0.05	18.4	9.5	0.6	1.4	0.2	Bal	N 0.05, Nb 0.07, V 0.2
253MA	0.09	20.9	10.9	0.6	1.6	0.3	Bal	N 0.19, Ce 0.04
800H	0.08	20.1	31.7	1.0	0.2	0.3	Bal	Al 0.4, Ti 0.3
333	0.05	25.0	45.0	-	1.0	3.0	18.0	Co 3.0, W 3.0
617	0.08	21.6	53.6	0.1	0.1	9.5	0.9	Co 12.5, Al 1.2, Ti 0.3
625	0.05	21.5	Bal	0.3	0.3	9.0	2.5	Nb 3.7, Al 0.2, Ti 0.2
602CA	0.19	25.1	62.6	0.1	0.1	-	9.3	Al 2.3, Ti 0.13, Zr 0.19, Y 0.09
230	0.11	21.7	60.4	0.5	0.4	1.4	1.2	W 14, Al 0.3, La 0.015
693	0.02	28.8	Bal	0.2	0.04	0.13	5.8	Al 3.3, Nb 0.67, Ti 0.4, Zr 0.03
740	0.07	25.0	Bal	0.3	0.5	0.5	1.0	Co 20.0, Ti 2.0, Al 0.8, Nb+Ta 2.0
718	-	19.0	52.0	-	-	3.0	19.0	Nb 5.0, Al 0.5, Ti 0.9, B 0.002
MA956	-	20.0	-	-	-	-	Bal	Al 4.5, Ti 0.5, Y_2O_3 0.6
WASP	0.02	20	Bal	0.5	0.75	4.3	2.0	Co 12-15, Ti 2.6-3.25, Al 1.0-1.5, Zr 0.1

different designs of the oxy-fuel systems and the types of coal targeted for combustion. We selected a SO_2 concentration of 0.99% for U.S. Eastern coal with a high sulfur content based on the premise that if the corrosion problems in a severe condition can be understood, then the issues in an environment with a low SO_2 content can be more easily resolved. Therefore, we conducted experiments to study alloy corrosion performance in an environment with a high SO_2 concentration simulating oxy-fuel combustion systems.

To understand the effect of gas composition on alloy corrosion, in the past, alloys were exposed to six different gas mixtures in the corrosion tests. The results from these exposures were reported at earlier conferences [1-4]. During the current year, we used two gas mixtures A and B, whose compositions are listed in Table 2. These gas mixtures contained the same concentrations of O_2 and SO_2, but A contained steam and B contained no steam. The effect of steam on the corrosion of alloys was studied by comparing the performance of the alloys in the gas environments with and without steam.

Table 2. Gas composition for experiments

Gas #	CO_2 (%)	H_2O (%)	O_2 (%)	SO_2 (%)
A	68.14	26.9	3.97	0.99
B	95.04	0	3.97	0.99

The US Eastern coal is rich in sulfur but contains a low concentration of CaO. In contrast, the calcium content in the U.S. Western coal is high, but its sulfur concentration is low. Our previous study on the ash corrosion of U.S. Eastern coal was performed in a gas environment with 0.99% SO_2. If the study of the high calcium ash on the alloy corrosion is performed in an environment with a low SO_2 concentration, the primary effect may be due to the difference of gas composition. To evaluate the effect of calcium in ash on corrosion, we used the same gas compositions for both studies on alloy performance in the presence of ash with and without high calcium concentration.

Synthetic Ash Experiments

The synthetic coal-ash deposit, which simulates ash from U.S. Eastern coal, consisted of a mixture of reagent-grade SiO_2, Al_2O_3, and Fe_2O_3 in a ratio of 1:1:1 according to weight. The alkali sulfate mixture consisted of Na_2SO_4 and K_2SO_4 in the ratio of 1:1 according to weight. The synthetic coal-ash deposit, which simulates ash from U.S. Western coal, consisted of a mixture of reagent-grade 36%SiO_2-16%Al_2O_3, 9%Fe_2O_3, and 29%CaO. Since coal ash generally forms at elevated temperatures (>1100°C) during combustion, these oxides can react with each other at the high temperatures. We also sintered these oxides at 1100°C in air, so that these oxides form phases similar to ash that forms during the combustion of coal. The alkali sulfate mixture consisted of Na_2SO_4 and K_2SO_4 at a 1:1 ratio by to weight. The ash contained 90% sintered oxides, and 10% sulfates (5%Na_2SO_4 + 5% K_2SO_4).

The specimens were buried in the ash, which was contained in an alumina boat. The experiments were generally stopped at approximately every 300 h, and the specimens were cooled to room temperature, cleaned of the ash by brushing, and weighed. Specimen exposures were then continued with a fresh supply of the ash mixture. The specimen temperature was controlled to within ≈3°C.

Upon completion of the corrosion kinetics experiments, the specimens were examined using optical metallography and by a scanning electron microscope (SEM) equipped with an energy-dispersive X-ray analyzer. In some cases, the deposit materials and the scales (which developed on the alloy specimens) were analyzed by X-ray diffraction (XRD). Optical examination of cross sections of exposed specimens and analyses with the SEM were used to identify the morphological features of corrosion-product phases in the scale layers and to establish the thickness of scales and depth of intergranular penetration, if any, in the alloys.

Results and Discussion

Corrosion experiments were conducted in the presence of ash with a high calcium concentration and alkali sulfates at 750°C in both Gas A and B for a total exposure time of 3600 h. Specimens were retrieved and weighed periodically and the ash was replenished after every 300 h of exposure. Figure 2 shows the weight loss data for all alloys tested in the presence of ash with a high calcium concentration and Gas A at 750°C. Since there are different elements in alloys, the reaction of these alloy constituents with ash chemicals are also different. Most alloys lost weight after exposure to the ash and oxy-fuel gas at 750ºC. However, Alloy 956MA and 718 gained weight initially because the reaction products adhered to the samples. Several alloys showed low weight loss during the tested period (Fig.2b), and many of the alloys exhibited an incubation period, during which the corrosion rate is low. Upon exceeding the incubation period, corrosion accelerated and the process followed a linear kinetics.

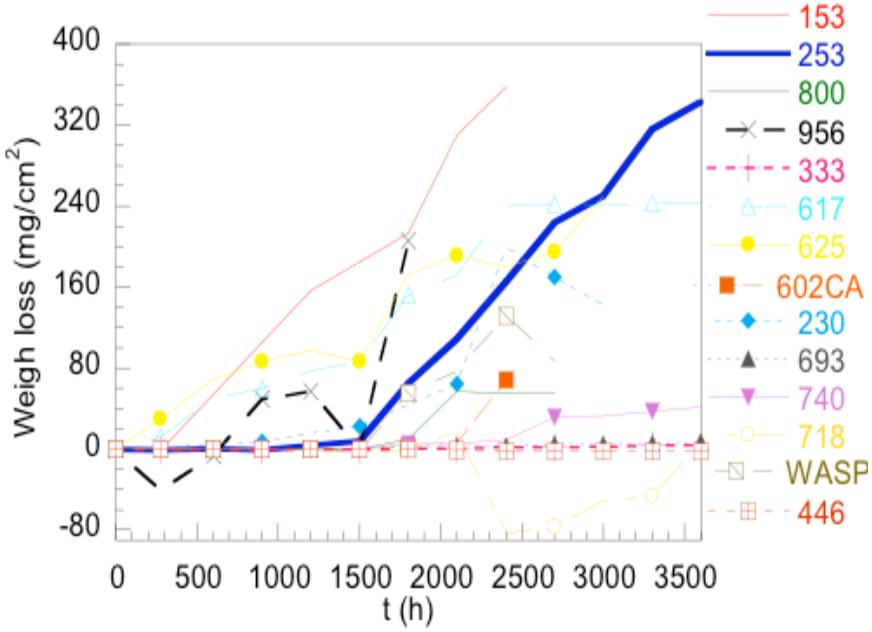

Figure 2a. Weight loss for alloys, after exposure to the synthetic ash with a high calcium concentration (simulating US Western coal) and Gas A at 750°C.

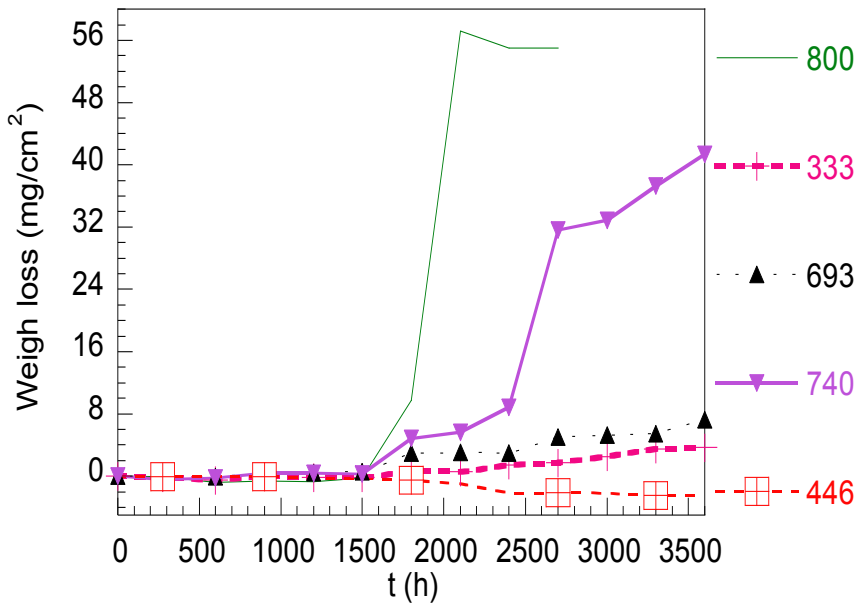

Figure 2b. Expanded view of Fig. 2a, weight loss for several alloys with low weight loss, after exposure to the synthetic ash with a high calcium concentration (simulating US Western coal) and Gas A at 750°C.

The effect of steam on the incubation time depends on the alloy composition and times can range widely based on the test results obtained in the environments with and without steam (see Fig. 3). In general, the incubation times for high Cr alloys such as 693 and 740, are long. The incubation times are short for alloys that contain Nb, W, and Mo. An addition of aluminum does not have a benefitial effect in ash corrosion.

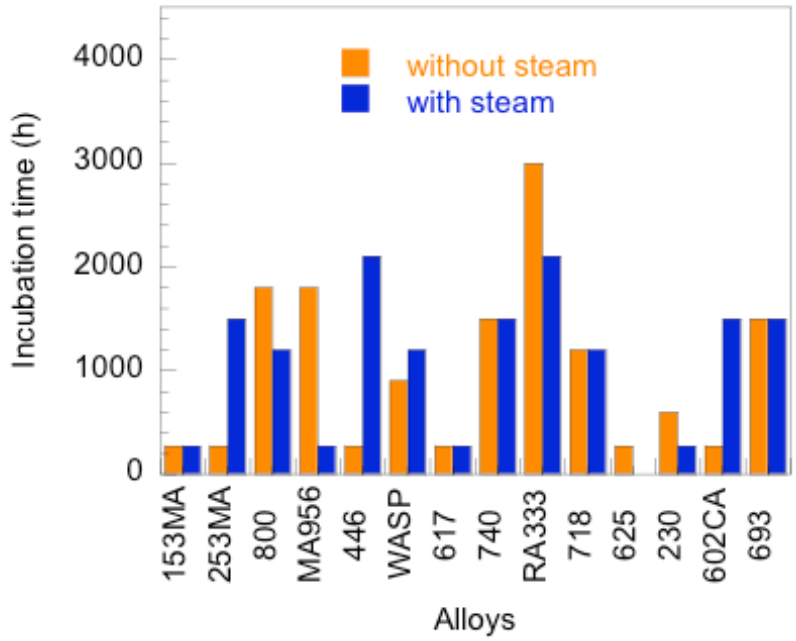

Figure 3. Incubation times for several alloys after exposure to the ash with a high calcium content (simulating US Western coal) plus alkali sulfates in Gas A (with steam) and Gas B (without steam) at 750°C.

The corrosion in some of the alloys, such as Alloy 602CA is localized when tested in the ash environment. Figure 4 shows that the localized attack on Alloy 602CA initiated at the right edge, and then the corrosion products grew outward. Although the weight loss may be low for such alloy samples, the local penetration rate of these alloys can be very high. In contrast, uniform corrosion was observed on Alloy 153MA. For coal power plants, penetration rates are more important than weight loss rates in the evaluation of long-term performance in the ash environment.

Figure 4. Photosgraphs of alloys after exposure to the ash with a high calcium content (simulating US Western coal) plus alkali sulfates in Gas B (without steam) at 750°C for 900h.

When compared to the lifetime of a coal power plant, an incubation period of several hundred to several thousand hours is relatively a short period. Since alloy materials have to be used for years in coal power plants, the long-term corrosion rate is important information to have for practical application. Therefore, it is necessary to obtain the corrosion rate beyond the incubation period even if it takes thousands of hours. Figure 3 indicates that many alloys exhibit an incubation period of 1000 h or more. Therefore, all the results from the short-term tests of 1000h or less are not adequate and may actually be false positive data for alloy selection for industrial application.

Figure 5 shows an example of the difference between a long-term test and a short-term test. The incubation period of Alloy 253 was approximately 1500h at 750°C in the ash with high calcium content (simulating US Western coal) plus alkali sulfates in Gas A. Figure 5C shows that the weight change rate was very low during the incubation period. Figure 5A also shows that the corrosion depth was small. If the 1200h test result is used to calculate the corrosion rate of this alloy, then a small rate of 0.31mm/y will be obtained.

However, if the test time exceeds the incubation period, the weight loss rate jumps and Figure 1B shows that the thickness of the sample was much less than its original thickness before the test. Using the corrosion depth of the 3600 h test, the corrosion rate jumped to 1.67mm/y when the incubation time was not subtracted. For long-term application, a 1500-h of incubation time is only a short period. The important parameter is the rate after the incubation period. Therefore, the right methodology for analyzing the ash corrosion data is to use the following equation to calculate the rate.

$$r = \frac{d}{t - IT} \tag{1}$$

where r is the long-term corrosion rate (in mm/year), d is corrosion depth (in mm). t is the total exposure time (in hours), and IT is the incubation time (in hours).

The rate calculated after the subtracting the incubation time was 2.87mm/y, which is over 9 times higher than the 1200-h short-term test result. We believe that this is the correct rate for long-term application of this alloy. This example shows that it is very important to test the candidate alloys long enough to exceed the incubation period and also use a valid methodology to analyze the data. Most previous reports and some of the ongoing work at other institutions on ash corrosion are based on results obtained from tests of 1000h or less duration. Since the incubation times of several of the alloys tested are longer than 1000h, the rates calculated from these tests are meaningless and won't represent the long-term corrosion performance of the alloys in coal-fired oxy-fuel plants..

Figure 6 shows the rates of corrosion penetration for alloys tested in the presence of ash with a high calcium content (simulating US Western coal) and Gas A and B at 750°C. The penetration rates of alloys after exposure to ash are much higher than those after exposure to the gas environment without ash [5]. In general, the linear penetration rates for the alloys ranged between 0.34 to 8.04 mm/y. Alloy 446 had the lowest penetration rate and Alloy 602CA had the highest rate. Alloy 740 also performed well. The corrosion rates of Fe-based alloys 153MA,

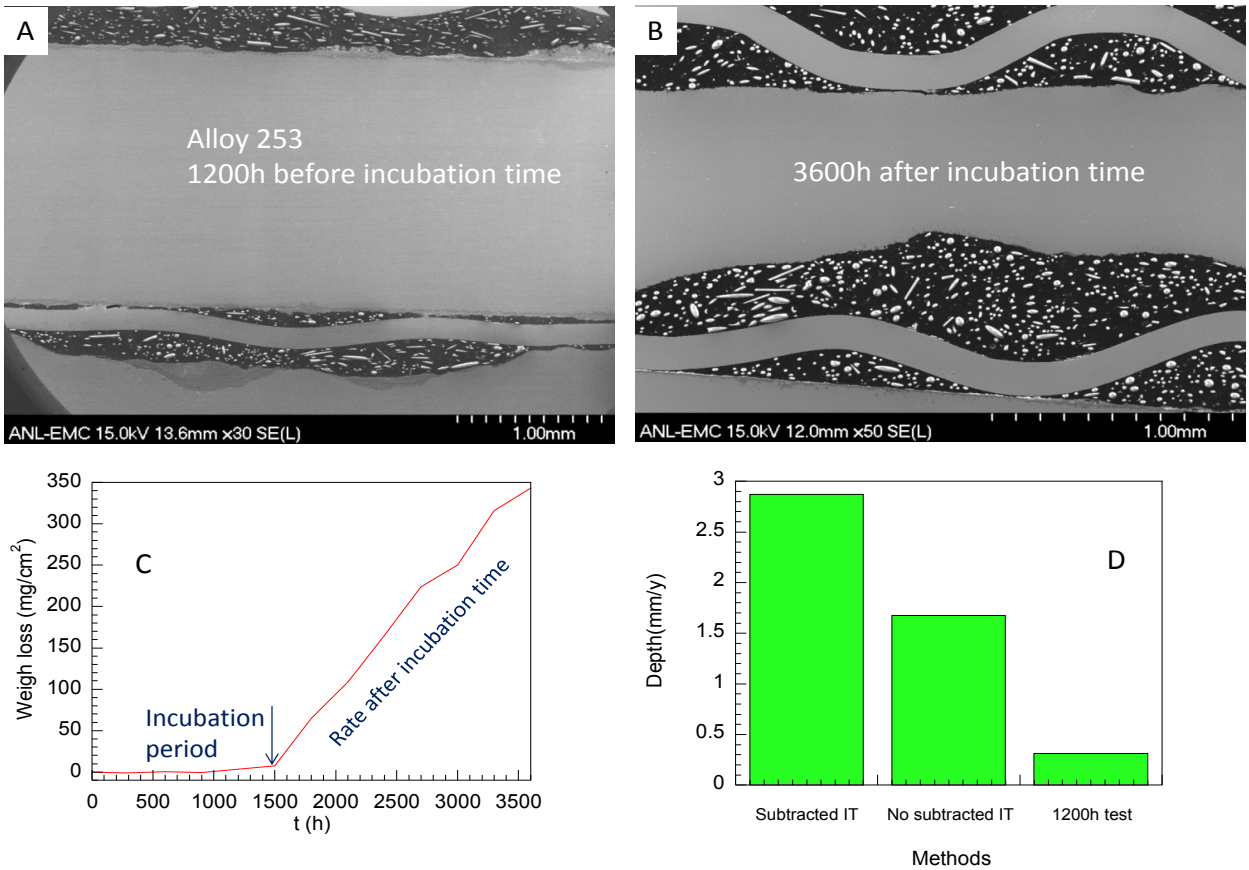

Figure 5. A: SEM cross section of Alloy 253MA after 1200h test at 750ºC in ash and oxy-fuel gas environment. B: SEM cross section of Alloy 253MA after 3600h test in ash and oxy-fuel gas environment. C: Weight loss of Alloy 253MA, after exposure to ash and oxy-fuel gas environment. D: Penetration rates of Alloy 253MA, calculated by different methods: subtracted incubation time (IT); not subtracted incubation time; and short time test data below incubation time.

253MA and MA956 are higher in the gas environment with steam than in the environment without steam. However, the rates of Ni-based alloys WASP, 617, 718, 625, and 230 are lower in the gas environment with steam than that without steam. The effects of gas chemistry on the corrosion rates are complicated, since the reactions of alloy constituents with ash and gas can vary widely.

A high Cr concentration >25% in alloys is necessary to resist ash corrosion at 750ºC. However, a high Cr concentration in an alloy cannot guarantee a low corrosion rate. For example, the corrosion rate for 602CA with 25.1wt% Cr is much higher than that of Alloy 617 with 21.6 wt% Cr. This shows the fact that ash corrosion is much more complicated than the corrosion without ash because of the multiple reactions between the ash and alloy constituents and gas species.

There are various strengthening elements in these alloys. For example, Alloys 740, 617, and WASP contain Co; Alloys 625, 617, WASP, 718, and 333 contain Mo; Alloy 230 and 333

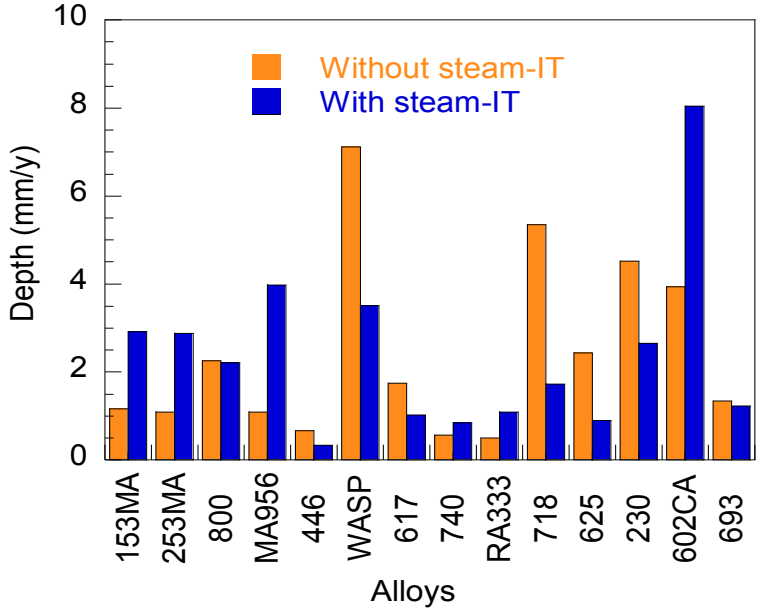

Figure 6. Corrosion depth rate data (after subtracting incubation time) for alloys after exposure to the ash with a high calcium content (simulating US Western coal) plus alkali sulfates in Gas A (with steam) and Gas B (without steam) at 750°C.

contain W; Alloys 718 and 625 contain Nb; Alloys MA956, 693, and 602CA contain Al. The elements in each alloy can react with ash and gas. The synergistic effects of these multiple reactions can also affect the corrosion rate. If compounds with low melting temperature could form, corrosion rate of the alloy will increase due to fluxing of the oxide layer on the alloy surface. It was reported that sulfates with low melting temperature could affect the corrosion rate. Table 3 shows melting temperatures of various sulfates and reaction products. The following reactions lead to low melting temperature sulfates:

$$Fe_2O_3 + 3K_2SO_4 + 3SO_3 = 2K_3Fe(SO_4)_3 \quad (2)$$
$$Fe_2O_3 + K_2SO_4 + 3SO_3 = 2KFe(SO_4)_2 \quad (3)$$
$$Fe_2O_3 + 3Na_2SO_4 + 3SO_3 = 2Na_3Fe(SO_4)_3 \quad (4)$$
$$Fe_2O_3 + Na_2SO_4 + 3SO_3 = 2NaFe(SO_4)_2 \quad (5)$$
$$Al_2O_3 + 3K_2SO_4 + 3SO_3 = 2K_3Al(SO_4)_3 \quad (6)$$
$$Al_2O_3 + K_2SO_4 + 3SO_3 = 2KAl(SO_4)_2 \quad (7)$$
$$Al_2O_3 + 3Na_2SO_4 + 3SO_3 = 2Na_3Al(SO_4)_3 \quad (8)$$
$$Fe_2O_3 + Na_2SO_4 + 3SO_3 = 2NaFe(SO_4)_2 \quad (9)$$
$$CoO + SO_3 = CoSO_4 \quad (10)$$
$$NiO + SO_3 = NiSO_4 \quad (11)$$

At 750°C and in an oxy-fuel gas environment, $CoSO_4$ and $NiSO_4$ are stable sulfates. However, $NaFe(SO_4)_2$, $NaAl(SO_4)_2$, $KFe(SO_4)_2$, $Na_3Fe(SO_4)_3$, and $Na_3Al(SO_4)_3$, are not stable. The stability of $K_3Fe(SO_4)_3$ depends on the gas composition. It has been reported that $K_3Fe(SO_4)_3$ and $KAl(SO_4)_2$ are responsible for the high temperature ash corrosion up to 760ºC [12,13]. However, the stability of $K_3Al(SO_4)_3$ is higher than $K_3Fe(SO_4)_3$ and $KAl(SO_4)_2$ [14, 15]. $K_3Al(SO_4)_3$ has also been identified by X-ray diffraction as constituents of corrosive-ash-deposit [16]. Most TGA and DSC analyses on $K_3Al(SO_4)_3$ were done in air. To understand the stability of $K_3Al(SO_4)_3$ in the oxy-fuel gas environment, a mixture of $K_2(SO_4)$, Al_2O_3, Fe_2O_3, and SiO_2

Table 3. Melting temperature of sulfates that could affect ash corrosion

Compound	Melting point (°C)
$Al_2(SO_4)_3$	770
$K_3Al(SO_4)_3$	654
$Na_3Al(SO_4)_3$	646
$K_3Fe(SO_4)_2$	618
$Na_3Fe(SO_4)_3$	624
$KFe(SO_4)_2$	694
$NaFe(SO_4)_2$	690
$CoSO_4$	735
$NiSO_4$-Na_2SO_4	671

with a molar ratio of 3:1:1:1 was reacted with Gas A at 750°C for 24h, and then quenched to room temperature to avoid the phase change during the furnace cooling process. X-ray diffraction confirms that the phase of $K_3Al(SO_4)_3$ can form at 750°C in an oxy-fuel gas environment (Figure 7). Pure $K_3Fe(SO_4)_3$ may not be stable at 750°C. However, part of $K_3Fe(SO_4)_3$ can dissolve into $K_3Al(SO_4)_3$ at 750°C. The concentration of $K_3Fe(SO_4)_3$ in $K_3Al(SO_4)_3$ will be determined by chemical equilibrium. It should be noted that the local concentration of SO_3 at the boundary of the ash/oxide scale on alloy surface can be much higher than that in the bulk gas due to the local catalytic reaction by Fe_2O_3 [17,18].

A thin dark layer between alloy substrate and oxide scale of Alloy 446 was observed (see the SEM image on Figure 8). EDX analysis indicated that the dark layer is the SiO_2 scale, which was developed by the outward diffusion of silicon from alloy substrate. There is another continuous layer of SiO_2 with thickness of ≈10μm on surface of Alloy 446 after exposure to Gas A at 750°C for 3600 h. EDX mapping shows that silicon and oxygen are the major elements in this layer. There is almost no iron or calcium in this layer., which indicates that it is not a simple ash layer that adheres to surface of alloy.

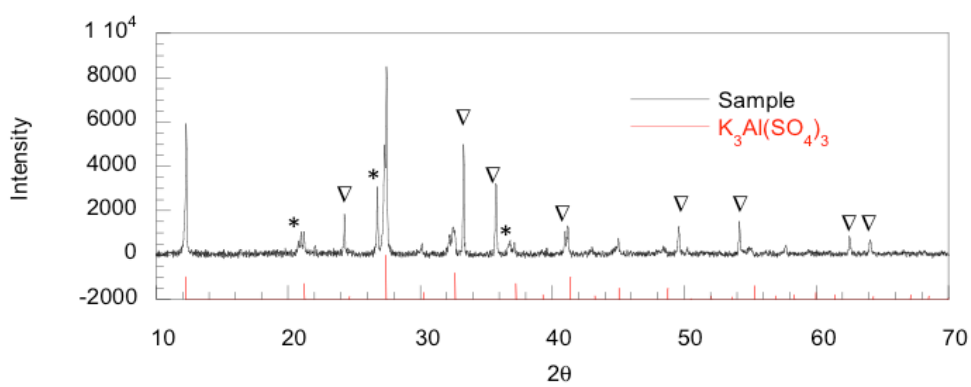

Figure 7. X-ray diffraction of the reaction product of a mixture of $K_2(SO_4)$, Al_2O_3, Fe_2O_3, and SiO_2 with a molar rate of 3:1:1:1 with Gas A at 750°C for 24h. The standard $K_3Al(SO_4)_3$ diffraction lines (PDF card # 00-027-1337) match the major diffraction peaks of the reaction product. Rest of the peaks in the XRD pattern correspond to Fe_2O_3(∇) and SiO_2 (*).

Alloy 446 does not contain aluminum, but outer layer after exposure contains a small amount of aluminum and a lot of silicon and the layer is a product of reactions of ash with alloy surface. The silica and alumina in the ash seems to deposit on the alloy surface whereas the scale that forms underneath the ash deposit consists of chromium/silicon oxide with virtual absence of Fe or Ni in scale. The calcium in the ash reacts with sulfur in the gas to form $CaSO_4$. Similar layer was also observed on surface of Alloy 740 at the protective region. In contrast, at the non-protective region, this layer is broken. The silicon oxide layer separates alloy surface from ash particles. It seems that this silicon oxide layer on alloy surface increased alloy's resistance to ash corrosion.

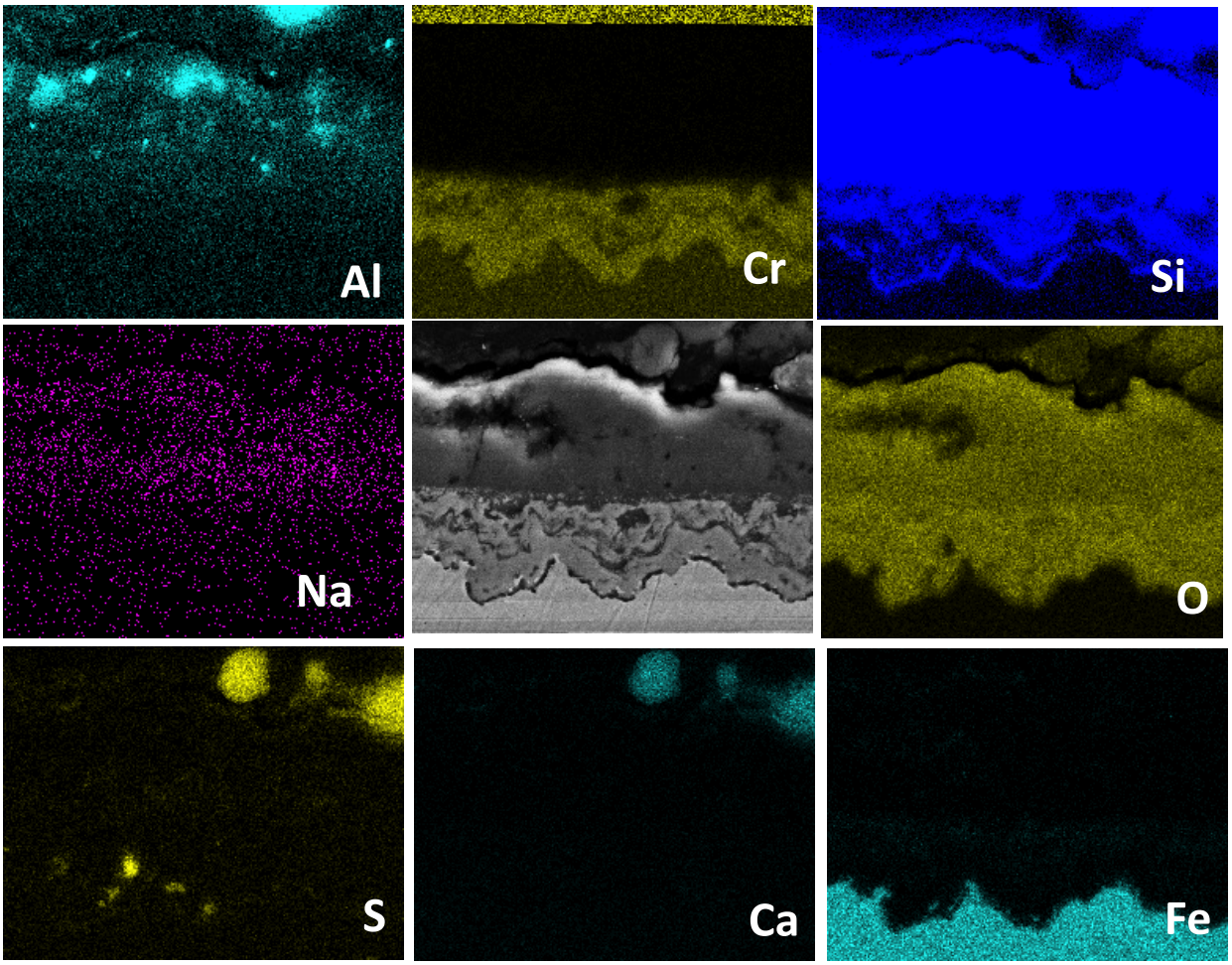

Figure 8. Energy-dispersive X-ray spectroscopies of the cross section of Alloy 446 after exposure to ash with high calcium content (simulating US Western coal) plus alkali sulfates in Gas A (with steam) at 750°C for 3600 h.

To understand the effect of calcium in ash on alloy corrosion, a comparison of corrosion performance of alloys is made from tests conducted with without calcium in the ash. Figure 9 shows that the incubation times for Alloys 253MA, 446, WASP, 740, RA333, 718, and 602CA are higher when they were exposed to ash with a high calcium content than to ash without calcium. However, the incubation time of Alloy 693 significantly decreased and the incubation

times of Alloy 153MA, 800, and 625 also reduced after exposure to ash with a high calcium content.

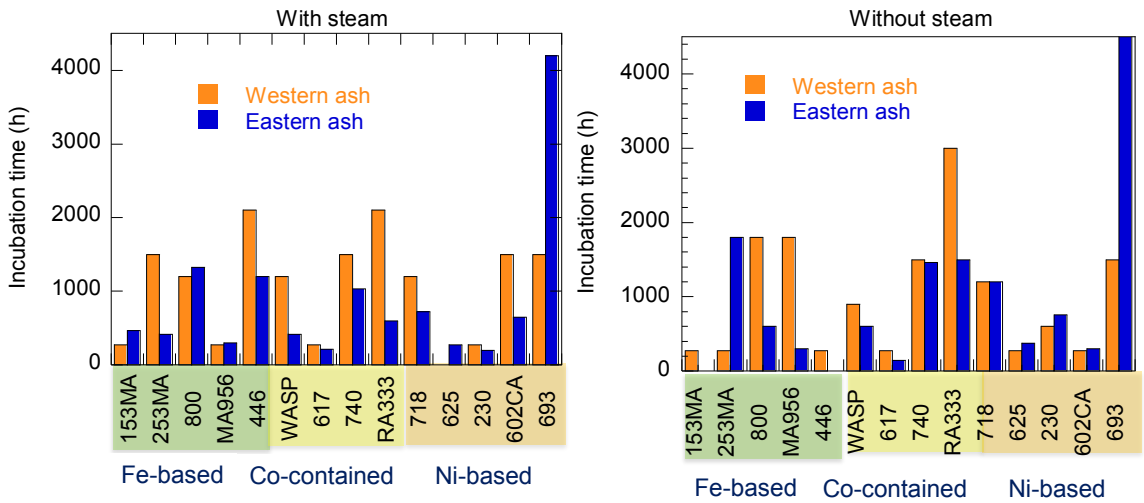

Figure 9. Incubation times of alloys after exposure at 750°C to ash with high calcium content (simulating US Western coal ash) and ash without calcium (simulating US Eastern coal ash) and to Gas A (left) and Gas B (right).

In coal combustion, the oxides in ash will be sintered at high combustion temperatures. However, limestone ($CaCO_3$) is also used as an additive in coal power plants to reduce the SO_2 concentrations in fuel gas. $CaCO_3$ can decompose to CaO at high temperatures. To understand the effect of CaO on the incubation time, we compared the alloy performance in the environments in ash with and without sintering. The ash without sintering contained free CaO and Al_2O_3, Fe_2O_3 and SiO_2. Figure 10A shows that alloys react with ash without sintering. The surfaces of Alloy 718, WASP, and 602CA have been obviously been attacked. Figure 11 shows that Alloy 693 was also attacked after exposure to this ash for only 300h. In contrast, the incubation time of Alloy 693 was longer than 3900h. Since the incubation time is sensitive to the surface condition, basic CaO can react with oxide scale to initiate localized corrosion. Thermochemical calculation also indicates that $CaCO_3$ and $CaSO_3$ can react with Cr_2O_3 in an oxide scale. However, if CaO reacted with SiO_2 to form calcium silicate in the sintering process, then the calcium silicate does not react with Cr_2O_3 in the oxide scale. Equation 15 shows that the free energy of such a reaction is positive.

$$CaO + Cr_2O_3 = CaCr_2O_4 \quad (12) \quad \Delta G = -58.7 \text{ kJ/mol at } 750°C$$
$$CaCO_3 + Cr_2O_3 = CaCr_2O_4 + CO_2 \quad (13) \quad \Delta G = -37.9 \text{ kJ/mol at } 750°C$$
$$CaSO_3 + Cr_2O_3 = CaCr_2O_4 + SO_2 \quad (14) \quad \Delta G = -16.9 \text{ kJ/mol at } 750°C$$
$$Ca_3Si_2O_7 + 3Cr_2O_3 = 3CaCr_2O_4 + 2SiO_2 \quad (15) \quad \Delta G = +69.7 \text{ kJ/mol at } 750°C$$

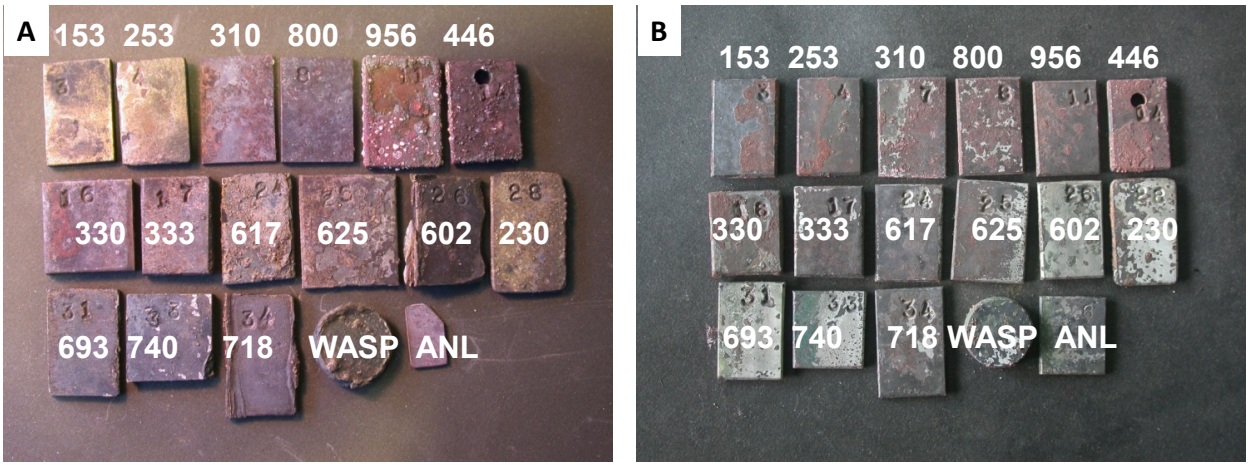

Figure 10. A: Photos of alloys after 300-h exposure at 750ºC to Gas B with the ash that the oxides (CaO, Al_2O_3, Fe_2O_3, and SiO_2) were not sintered before exposure of the alloys.
B: Photos of alloys after 300-h exposure at 750ºC to Gas B with the ash that the oxides (CaO, Al_2O_3, Fe_2O_3, and SiO_2) were sintered before mixing with K_2SO_4 and Na_2SO_4 and exposure of the alloys.

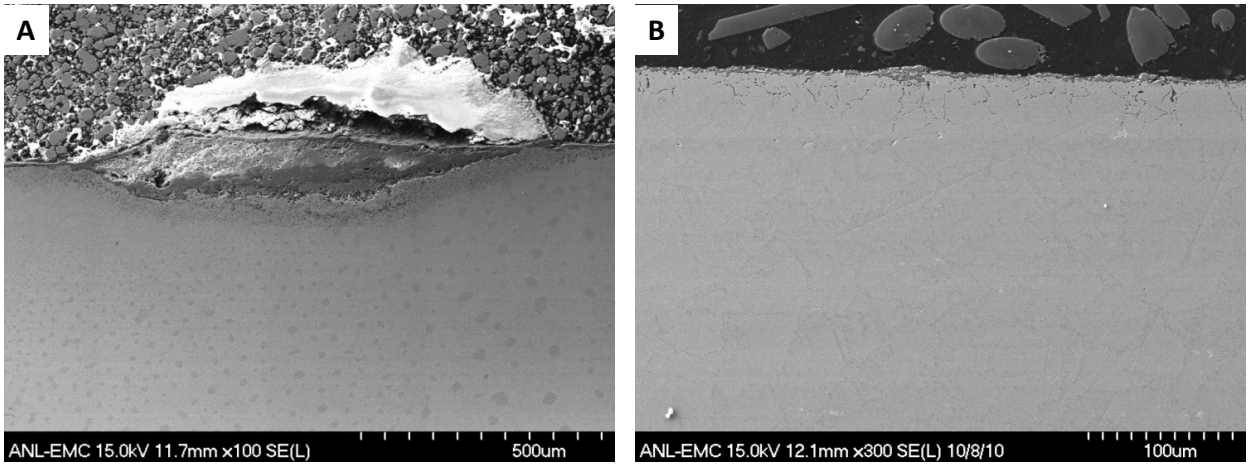

Figure 11. A: SEM cross section image of Alloy 693 after 300-h exposure at 750ºC to Gas B with ash in which the oxides (CaO, Al_2O_3, Fe_2O_3, and SiO_2) were not sintered before exposure of the alloys.
B: SEM cross section image of Alloy 693 after 600-h exposure at 750ºC to Gas B with the ash without calcium.

X-ray diffraction indicated that $CaSiO_3$, $Ca_3Si_2O_7$, and other calcium aluminosilicates form upon sintering the oxide mixture (CaO, Al_2O_3, Fe_2O_3, and SiO_2) at 1100ºC for 24h. These silicates are stable compounds at 750ºC. Figure 10B shows that the reactions of alloys with the sintered ash are much less than with the ash without sintering. After sintering, CaO reacted with SiO_2 and other oxides in the ash. The attack of CaO on the alloy surface was minimized. Figure 6 shows that the incubation times of some alloys such as 253MA, 446, 740, RA333, and 602CA, that were exposed to the sintered ash with a high calcium content were longer than the incubation

time of alloys exposed to ash without calcium. This experiment indicates that the methods that introduce limestone or other calcium additives into a coal combustion facility can affect the incubation time of alloy materials.

Compared to the lifetime of a coal combustion facility, the incubation time is only a short period. The long-term corrosion rate after the incubation time is more important. Figure 12 shows that the long-term corrosion rates of most alloys were lower after exposure to the ash with a high calcium content than to the ash without calcium. Therefore, high calcium content in ash can reduce long-term corrosion rates. The corrosion rate of Alloy 740, which was exposed to ash with a high calcium content decreased to 0.84mm/year from 1.2 mm/y compared to the alloy that exposed to ash without calcium. The corrosion rate (0.34mm/y) of Fe-based Alloy 446 was the lowest among these alloys.

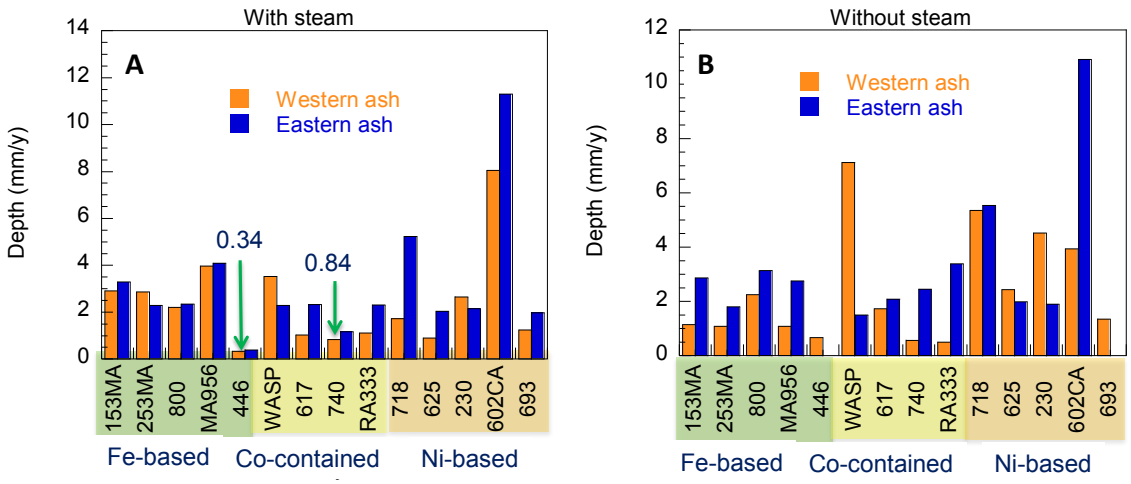

Figure 12. A: Long-term corrosion rates after subtracted incubation times of alloys after exposure at 750ºC to Gas A and the ash with a high calcium content (simulating US Western coal ash) and the ash without calcium (simulating US Eastern coal ash).
B: Long-term corrosion rates after subtracted incubation times of alloys after exposure at 750ºC to Gas B and the ash with a high calcium content (simulating US Western coal ash) and the ash without calcium (simulating US Eastern coal ash).

Since the gas composition and the other furnace parameters were the same, the decreasing corrosion rates of alloys should be due to only the effect of the calcium in the ash. The reactions of the calcium compounds in ash and other corrosion products may affect the corrosion rate. The ash with a high calcium content and without calcium were analyzed by X-ray diffraction after exposure to Gas A at 750°C for 300h. Figure 13 shows the XRD analysis results. $K_3Al(SO_4)_3$, Al_2O_3, Fe_2O_3, and SiO_2 were identified in the ash without calcium. EDX analysis also indicated that K, Al, and S stay together with O at the EDX mapping of the corroded region on Alloy 446 after exposure to the ash without calcium (simulating US Eastern coal) plus alkali sulfates in Gas A (with steam) at 750°C for 5100 h (Figure 14). $Al_3Fe_5O_{12}$ is also possible to present as a minor phase. In contrast, there was not the $K_3Al(SO_4)_3$ phase in the ash with a high calcium content after exposure to the same Gas A at 750°C for 300h. $K_3Al(SO_4)_3$ melts at 654°C. Oxide scales can dissolve into molten salt, which leads to fast corrosion. After a reaction with SO_2 and oxygen in Gas A, most of calcium in the ash was converted to $CaSO_4$. K_2SO_4 and $CaSO_4$ can

form a compound of $K_2Ca_2(SO_4)_3$. Sodium may be substituted for potassium in $K_2Ca_2(SO_4)_3$ to form a solid solution of $(K, Na)_2Ca_2(SO_4)_3$. A small amount of the $CaSiO_3$ phase was still observed in the ash with a high calcium content after exposure to Gas A at 750°C for 300h. $CaSiO_3$ can react with $K_3Al(SO_4)_3$, $CoSO_4$ and $NiSO_4$.

$$6CaSiO_3 + 4K_3Al(SO_4)_3 = 3K_2Ca_2(SO_4)_3 + 3K_2SO_4 + 2Al_2O_3 + 6SiO_2 \quad (16)$$
$$CaSiO_3 + CoSO_4 = CaSO_4 + CoSiO_3 \quad (17)$$
$$CaSiO_3 + NiSO_4 = CaSO_4 + NiSiO_3 \quad (18)$$

The melting temperature of CoSO4 is 735°C, and NiSO4 can also form a low melting temperature mixture with Na2SO4 (see Table 3). The formation of these phases with a low melting temperature was considered to lead to fast corrosion. However, these low melting point phases cannot form if there is CaSiO3 in the ash. Therefore, calcium silicates and calcium aluminosilicates in ash can retard the formation of some low melting point sulfates that can lead to fast corrosion.

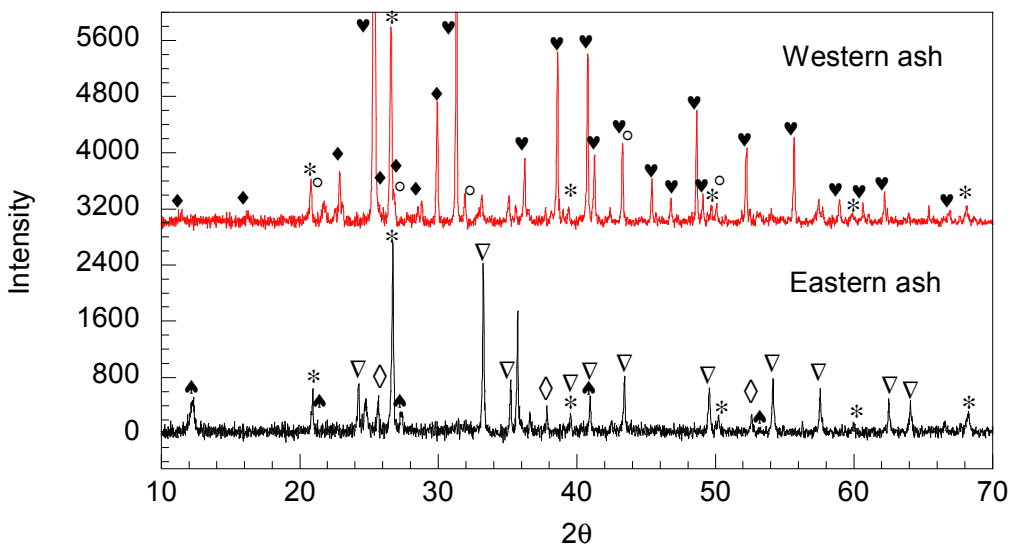

Figure 13. X-ray diffraction of simulated Eastern and Western ashes after exposure to Gas A at 750°C for 300h. ♥: $CaSO_3$; ♠: $K_3Al(SO_4)_3$; *: SiO_2; °: $K_2Ca_2(SO_4)_3$;∇: Fe_2O_3; ◊: Al_2O_3

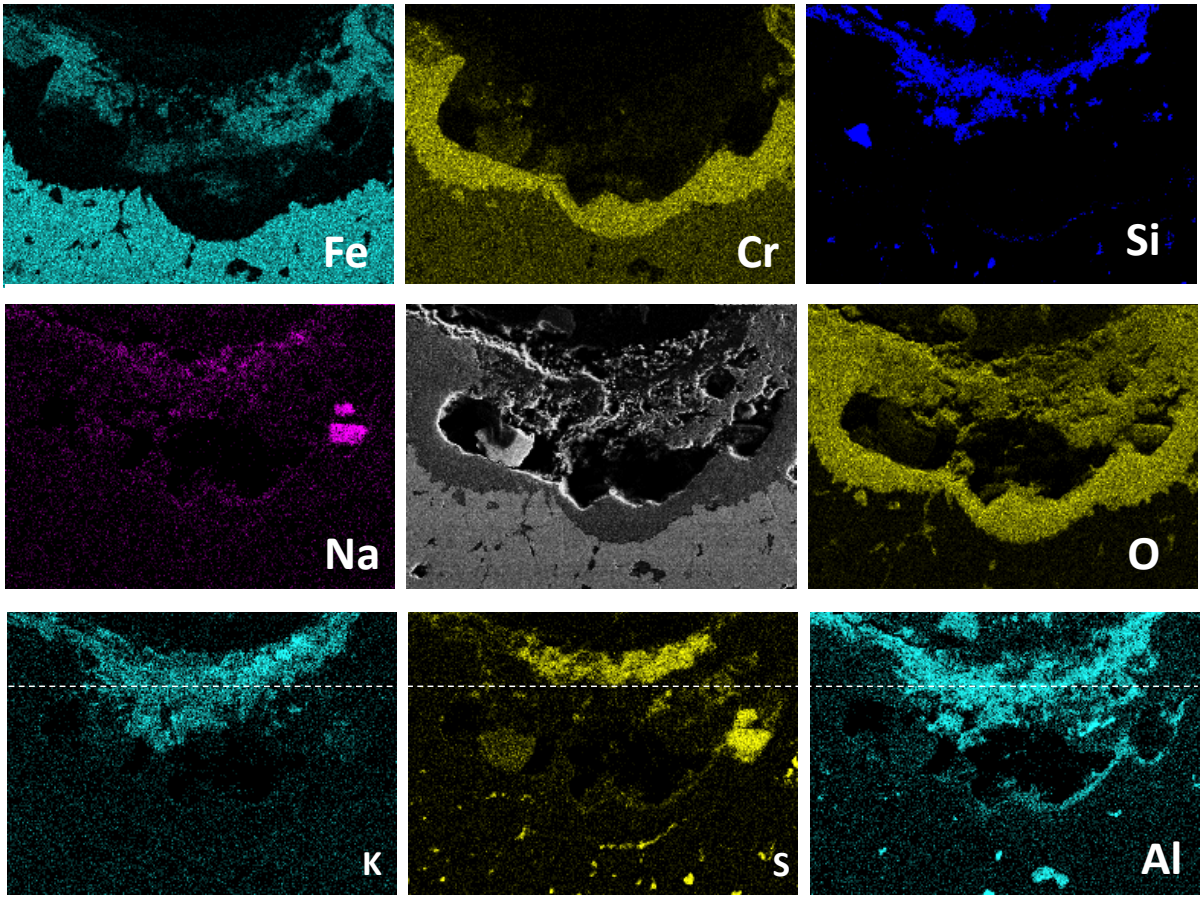

Figure 14. Energy-dispersive X-ray spectroscopies of the cross section of Alloy 446 after exposure to the ash without calcium (simulating US Eastern coal) plus alkali sulfates in Gas A (with steam) at 750°C for 5100 h.

The current study indicates that the corrosion rates of some alloys such as Alloy 740 were lower in an environment with ash containing a content of calcium (simulating US Western coal ash) than in an environment with ash without calcium (simulating U.S. Eastern coal ash) even though the corrosion tests were performed in the gas with the same composition. The sulfur content in U.S. Western coal is much less than in U.S. Eastern coal. Therefore, the SO_2 content in flue gas from the combustion of US Western coal will also be less than in the flue gas from the combustion of US Eastern coal. It has been reported that the ash corrosion rates of alloys in the gas environment with a low SO_2 concentration are lower than in the gas with a high SO_2 concentration [19]. Therefore, it is expected that the corrosion rate of alloys will be further lowered, if the alloys are exposed to Western ash with a high calcium content and a lower SO_2 concentration in the flue gas.

It has been reported that a high SO_2 concentration in oxy-fuel combustion increases the efficiency of in-furnace desulfurization and leads to a higher conversion of SO_2 to other sulfur species because the decomposition of $CaSO_4$ is retarded by a high SO_2 concentration in furnaces [20, 21]. However, higher concentrations of SO_2 can lead to increased ash corrosion. If an

external SO_2 removal process has to be used to decrease the SO_2 concentration in the combustor (especially with recycled gas) to avoid ash corrosion, it becomes more difficult and expensive. The current study reveals that it is possible to reduce the ash corrosion rates of alloys in oxy-fuel gas environments by using additives such as Ca compounds, to change the chemical composition of the ash. Our test results confirm a possible alternate approach to reducing the alloy corrosion rate in oxy-fuel combustion systems.

The performance of Alloy 740 with a low Fe content was the best among the Ni-based alloys. Alloy 446 contains almost no Ni or Co, and therefore, low melting sulfates of Co and Ni would not form on the alloy surface to flux the oxide scale. Since Alloy 446 has low strength at elevated temperatures, it needs to be used as a cladding or coating to minimize corrosion of structural alloys in oxy-fuel environments.

Summary

We have conducted a detailed study at Argonne National Laboratory, to evaluate the corrosion performance of structural alloys at 750°C in simulated oxy-fuel environments in the presence of synthetic ash and sulfur-containing gaseous environments. Ash with a high calcium content (simulating US Western coal ash) and the ash without calcium ash (simulating US Eastern coal ash) were used in this study. The performance of the alloys after exposure to the two ashes was compared. The results showed that calcium in ash can affect both the incubation time and the long-term corrosion rate of alloys. Adding CaO to ash without sintering can reduce the incubation times of alloys because CaO or $CaCO_3$ can react with the oxide scale to initiate localized corrosion. Upon sintering, CaO reacts with SiO_2 and other oxides in the ash to form stable silicates or aluminosilicates, the attack due to CaO on the alloy surface is minimized. On the other hand, calcium silicates and/or aluminosilicates can retard the formation of some low-melting-point sulfates that can lead to rapid corrosion. Experimental results indicate that the long-term ash corrosion rate of alloys that are exposed to oxy-fuel gas and ash with a high calcium content at 750°C can be lower than that exposed to the same gas and temperature but using ash without calcium. The long-term ash corrosion rate of Alloy 740 is reduced to below 1 mm/y after increasing the calcium content in the ash. The corrosion rate of the Fe-based Alloy 446 is the lowest among all alloys. This alloy may be a good candidate for coating or cladding of the structural alloys to resist ash corrosion in oxy-fuel gas environments at 750°C. The test results indicate that it is promising to solve the ash corrosion problem in the oxy-fuel gas environment by using alloy selection, applying additives, and cladding or coating methods.

Acknowledgements

This paper was presented at the 27th Annual Conference on Fossil Energy Materials, Pittsburgh, PA, June 18-20, 2013. This work was supported by the U.S. Department of Energy, Office of Fossil Energy, Advanced Research Materials Program, Work Breakdown Structure Element ANL-4, under Contract DE-AC02-06CH11357. The authors would like to thank Robert Romanosky and Patricia Rawls of NETL for their support. Use of the Advanced Photon Source, the Center for Nanoscale Materials, and the Electron Microscopy Center for Materials Research were supported by the U.S. Department of Energy, Office of Science, Office of Basic Energy Sciences, under Contract DE-AC02-06CH11357.

References

1. K. Natesan and D. L. Rink, "Corrosion Performance of Structural Alloys for Oxy-fuel Combustion Systems," Proc. 21st Annual Conference on Fossil Energy Materials, Knoxville, TN, April 30-May 2, 2007 and published in the conference proceedings.

2. K. Natesan, Z. Zeng, and D. L. Rink, "Materials Performance of Structural Alloys in CO_2 and in CO_2-Steam Environments," Proc. 22nd Annual Conference on Fossil Energy Materials, Pittsburgh, PA, June 8-10, 2008 and published in the conference proceedings.

3. K. Natesan, Z. Zeng, and D. L. Rink, "Materials Performance of Structural Alloys in CO_2 and in CO_2-Steam Environments," paper presented at the 23rd Annual Conference on Fossil Energy Materials, Pittsburgh, PA, May 12-14, 2009 and published in the conference proceedings.

4. K. Natesan, Z. Zeng, and D. L. Rink, "Materials Performance of Structural Alloys in Simulated Oxy-fuel Environments," paper presented at the 24rd Annual Conference on Fossil Energy Materials, Pittsburgh, PA, May 25-27, 2010 and published in the conference proceedings.

5. K. Natesan, Z. Zeng, and D. L. Rink, "Effect of Gas Composition on Materials Performance of Structural Alloys in Simulated Oxy-fuel Environments," paper presented at the 25th Annual Conference on Fossil Energy Materials, Portland, OR, April 26-28, 2011 and published in the conference proceedings.

6. K. Natesan, and Z. Zeng, "Role of Coal Ash in the Corrosion Performance of Structural Alloys in Simulated Oxy-Fuel Environments," Proceedings of 26th Annual Conference on Fossil Energy Materials, Pittsburgh, PA, April 17-19, 2012 and published in the conference proceedings.

7. L. Elliott, T. Wall, S. Khan, R. Rathnam, Y. Liu, R. Gupta, "Pilot scale studies to support oxy-fuel feasibility study: advanced analyses, mathematical modeling and interpretation of results," ACARP: The University of Newcastle; 2006.

8. T. Suko, T. Yamada, M. Tamura, T. Fujimori. In: I.-H.H.I.C.L. (IHI), editor. Pilot Scale studies to support oxy-fuel feasibility, Cooperative Research Center for Coal in Sustainable Development (CCSD), 2006.

9. S. Schnurrer, L. Elliott, T. Wall. Influence of oxy-fuel environment on sulphur species in ash from pulverised coal combustion, In: 7th International symposium on gas cleaning at high temperatures. 2008: Shoal Bay, NSW Australia.

10. G. Stein-Brozozowska, J. Maier, G. scheffknecht, Impact of the oxy-fuel combustion on the corrosion behavior of advanced austenitic superheater materials, Energy procedia, 4, 2035-42, 2011.

11. A. Robertson, H, Agarwal, M. Gagliano, and A. Seltzer, Oxy-combustion boiler materials development, The 37th International technical conference on clean coal & fuel systems, Clearwater, Florida, June 3, 2012.

12. Elmer John Badin, Coal combustion chemistry-corrosion aspects, Elsevier, 1984.

13. Babcock&Wilcox, Steam/its generation and use, The Babcock&Wilcox Company, 1978.

14. A. Kucuk and M. S. Gulaboglu, Thermal decomposition of saphane alunite ore, Ind. Eng. Chem. Res., 41, 6028-32, 2002.

15. W. W. Rudolph, R. Mason, and P. Schmidt, Synthetic alunites of the potassium-oxonium solid solution series and some other members of the group: synthesis, thermal and X-ray characterization, Eur. J. Mineral, 15, 913-24, 2003.

16. Cain C. Nelson W. Corrosion of superheaters and Reheaters of pulverized-coal-fire boiler, II. J. Eng. Power: Series A, 1961, 83: 468-74.

17. C.H. Anderson, C.W. Goddard, J. Inst. Fuel, 41, 357, 1968.

18. H.H. Kraus, A. Levy, WT. Reid, Tans ASME Ser A, J. Eng. Pwr. 91, 216, 1969.

19. N. Otsuka, Fireside corrosion of austenitic tube materials for advanced USC Boilers, Mater. Sci. Forum, 696, 206-11, 2011.

20. H. Liu, S. Katagiri, and K. Okazaki, Drastic SO*x* Removal and Influences of Various Factors in O_2/CO_2 Pulverized Coal Combustion System, Energy & Fuels, 15, 403-412, 2001.

21. R. Stanger and T. Wall, Sulphur impacts during pulverised coal combustion in oxy-fuel technology for carbon capture and storage, Progress in Energy and Combustion Science, 37, 79-88, 2011.